**Title**
Hyperpolarized 13C MR for Molecular Imaging of Prostate Cancer



**Journal**
Journal of Nuclear Medicine, 55(10)

**ISSN**
0161-5505

**Authors**
Wilson, David M
Kurhanewicz, John

**Publication Date**
2014-10-01

**DOI**
10.2967/jnumed.114.141705

Peer reviewed

HHS Public Access

Author manuscript

*J Nucl Med*. Author manuscript; available in PMC 2015 March 04.

Published in final edited form as:

*J Nucl Med*. 2014 October ; 55(10): 1567–1572. doi:10.2967/jnumed.114.141705.

# Hyperpolarized $^{13}$C MR for Molecular Imaging of Prostate Cancer

**David M. Wilson** and **John Kurhanewicz**

Department of Radiology and Biomedical Imaging, University of California San Francisco, San Francisco, California

## Abstract

Hyperpolarization using dissolution dynamic nuclear polarization has emerged as a versatile method to dramatically improve the MR signal of low-sensitivity nuclei. This technique facilitates the study of real-time metabolism in vitro and in vivo using $^{13}$C-enriched substrates and has been applied to numerous models of human disease. In particular, several mechanisms underlying prostate cancer have been interrogated using hyperpolarized $^{13}$C MR spectroscopy. This review highlights key metabolic shifts seen in prostate cancer, their study by hyperpolarized $^{13}$C MR spectroscopy, and the development of new platforms for metabolic study.

### Keywords

PET/MR imaging; PET/MRI; $^{13}$C-magnetic resonance; prostate; prostate cancer; hyperpolarized $^{13}$C; metabolism

The recent first-in-man hyperpolarized $^{13}$C MR imaging study in prostate cancer patients has confirmed the clinical potential of this remarkable technology (1). Hyperpolarization using dynamic nuclear polarization (DNP) is now a robust technique used to dramatically increase the signal-to-noise ratio of nuclei that have a spin of one half. This increased sensitivity has facilitated the study of chemical phenomena in solution and the probing of a variety of metabolic pathways in vitro and in vivo (2). The technique is particularly sensitive to the metabolic reprogramming that occurs in malignancy and has been applied to several cell and animal models of prostate cancer.

Prostate cancer is now the most commonly diagnosed cancer in men in the United States, with an estimated 233,000 new cases of the disease in 2014 (3). The landscape of the disease is changing rapidly, motivating new therapeutic and diagnostic approaches. There is considerable debate about prostate cancer management, based on the efficacy of common treatments (most commonly antiandrogen therapy, radiotherapy, and radical prostatectomy), side effects, and recent progress in the understanding of prostate cancer biology. Radical prostatectomy remains the most frequently recommended treatment for patients with a life



For correspondence or reprints contact: John Kurhanewicz, Department of Radiology and Biomedical Imaging, 1700 4th St., Byers Hall 203, San Francisco, CA 94158. john.kurhanewicz@ucsf.edu.

**DISCLOSURE**

This work was supported by the National Institutes of Health (R01 CA166766, P41 EB013598). No other potential conflict of interest relevant to this article was reported.

expectancy of greater than 10 y but has severe side effects, including erectile dysfunction and urinary incontinence. Expectant management, or watchful waiting, may be the answer for patients in whom disease is likely to be indolent. However, the diagnostic tools needed to predict disease aggressiveness are lacking, making patient-specific therapy difficult.

These difficulties are highlighted by therapies targeting the androgen receptor. Androgen deprivation therapy is currently a mainstay of prostate cancer treatment, with androgen antagonists (e.g., bicalutamide) prescribed as monotherapy or in conjunction with other therapies. Recently, two highly potent antiandrogen agents have been approved, namely the androgen receptor antagonist enzalutamide and the androgen biosynthesis inhibitor abiraterone acetate (4,5). A durable response to these agents is not universal, with relapse occurring in a significant subset of patients within 1 y. Furthermore, there is a small but provocative body of evidence that potent, chronic androgen receptor inhibition can drive transformation to androgen-independent neuroendocrine prostate cancer (6,7). This treatment-induced evolution of neuroendocrine prostate cancer (also known as small cell carcinoma) from adeno-carcinoma is thought to be an adaptive response with an increasing incidence in the clinic. Metabolic markers of this transition are urgently needed to treat patients receiving antiandrogen therapy appropriately.

The development of neuroendocrine prostate cancer in patients receiving androgen receptor therapy is just one example of the numerous ways prostate cancer can evade therapy, escape detection, and behave in unpredictable ways. Increasingly, cancer is considered a metabolic disease, with the metabolic shifts enforced by oncogenes and tumor suppressors (8). This concept differs from the traditional view of cancer as a primarily genetic, proliferative phenomenon. The focus of this mini review is identification of several of the metabolic shifts seen in cancer that may be exploited for diagnostic purposes, in particular by the agents and platforms developed for hyperpolarized $^{13}C$ MR spectroscopy (MRS).

## TARGETING METABOLISM: THE SEARCH FOR NEW IN VIVO BIOMARKERS

A snapshot of prostate cancer metabolism is frequently obtained via $^{1}H$ MRS, acquired in conjunction with anatomic data during a prostate MR imaging scan. MRS significantly improves the local evaluation of prostate cancer presence and volume, particularly when performed at higher field-strengths (3T) in conjunction with other functional MR methods, namely dynamic contrast-enhanced imaging and diffusion-weighted imaging. Three-dimensional MR spectroscopic imaging (MRSI) allows metabolic mapping of the entire prostate gland, whereby resonances corresponding to citrate, creatine, choline, and polyamines may be visualized. Changes in the concentrations of these metabolites can be used to identify cancer with high specificity. The spectra taken from regions of prostate cancer show significantly reduced or absent citrate and polyamines, whereas choline is elevated relative to spectra taken from surrounding healthy tissue. These changes in citrate are attributed to a shift from citrate-producing to citrate-oxidizing metabolism (9). The total choline resonance is increased by numerous mechanisms, including overexpression and activation of choline cycle enzymes (10). Therefore, the choline-to-citrate ratio ([choline + creatine]/citrate) is commonly used for spectral analysis since the choline and creatine peaks

are poorly resolved. The metabolic reprogramming seen in prostate cancer, as well as a characteristic $^{1}$H MRSI scan, are depicted in Figure 1.

The development of hyperpolarized $^{13}$C MRS, and its recent application to prostate cancer patients, have significantly expanded metabolic targets for imaging. Metabolic shifts in cancer are too numerous to describe in full here but include accelerated aerobic glycolysis, increased consumption of glutamine, and redox adaptation, whereby cancer cells accumulate intracellular antioxidants. These metabolic shifts are enforced by oncogenes (most notably PI3K/AKT, MYC, and HIF-1) and the loss of tumor suppressor genes such as P53. The following summaries are offered to suggest how these transitions may be exploited by new metabolic imaging technologies.

## The Warburg Hypothesis: The Glycolytic Phenotype

The pioneering studies of Otto Warburg were reported in 1926, describing the altered metabolism of tumors. These studies reported the remarkable preference of tumors for aerobic glycolysis, whereby the pyruvate produced by glycolysis is converted to lactate, rather than entering the tricarboxylic acid cycle. This preference for fermentation exists even when $O_2$ is present—a surprising result indeed: why would a tumor cell prefer the 2 adenosine triphosphates generated by glycolysis to the 36 adenosine triphosphates afforded by complete oxidation of glucose? This preference may represent the selection of cells adapted to hypoxia, given the tendency of tumors to outgrow their blood supply. Alternatively, suppression of reactive oxygen species formed during oxidative phosphorylation likely represents another adaptive mechanism. The “why” remains controversial, but the Warburg phenotype has proved particularly useful in the detection of cancers, which are largely glucose-avid. PET scans using $^{18}$F-FDG are currently the standard detection method for identifying meta-static disease in the body for a variety of human cancers. However, $^{18}$F-FDG PET offers poor tissue contrast in the prostate, and its use is complicated by proximity to the excretory system. Furthermore, the fundamental switch in prostate cancer is altered carbon use, not just glucose uptake. Therefore, use of fast $^{13}$C MR after injection of hyper-polarized [1-$^{13}$C]pyruvate to measure this metabolic switch and its relationship to cancer aggressiveness and therapeutic response makes biologic sense.

The shunting of pyruvate, an end product of glycolysis, to lactate in tumor is facilitated by increased expression of lactate dehydrogenase, as well as expression of monocarboxylate transporters that have a role in both monocarboxylate uptake and, significantly, lactate export (11,12). In particular, monocarboxylate transporter 4 is a high-affinity lactate transporter that cotransports lactate and a proton out of the cell, contributing to acidification of the extracellular matrix. Lactate dehydrogenase has been explored as an anticancer target, with decreased expression in xenograft models resulting in lowered tumorigenicity (13).

## A Glutamine Addiction?

Several cancers increase glutamine consumption through induction of glutamine transporters, as well as enhanced expression of enzymes that metabolize glutamine, namely glutaminases and glutamate oxaloacetate transaminases. In some cancer cells, withdrawal of

glutamine results in cell death. Enhanced glutamine metabolism is believed to be a compensatory mechanism related to the flow of citrate out of the tricarboxylic acid cycle, needed to provide acetyl-CoA for fatty acid biosynthesis. Mitochondrial citrate can either undergo oxidation in the mitochondria (via aconitase) to isocitrate or be exported into the cytosol for lipogenesis. Glutamine, converted to α-ketoglutarate, thus provides an essential carbon source for the tricarboxylic acid cycle in the tumor metabolic phenotype. This altered metabolism may be driven by c-MYC, a transcription factor whose deregulation is common in cancer. MYC has been shown to induce both the expression of glutamine transporters and upregulation of glutaminases (14,15).

### Redox Adaptation

Radiation therapy, with or without concomitant hormonal therapy, is a mainstay of prostate cancer therapy. Of newly diagnosed prostate cancer patients, approximately 30% have high-risk disease (stage T3–T4 or prostate-specific antigen level > 20 μg/L or Gleason score of 8–10) and are at risk for biochemical and clinical failure after therapy (16). Even with modern conformal radiation therapy, treatment failure occurs in approximately 45% of patients with locally defined disease (17). Increasingly, redox (reduction and oxidation) mechanisms are considered critical in radiation resistance (18). The cytotoxic effect of radiation therapy is mediated by generation of reactive oxygen species in tissues, which cause oxidative damage in DNA, proteins, and lipids, leading to DNA strand breaks, loss of protein function, and membrane damage. Recently, it has been demonstrated that reduced nicotinamide adenine dinucleotide phosphate oxidase enzymes are upregulated in response to androgens, stimulating the production of stress molecules and antioxidative enzymes; inhibition of these enzymes sensitizes human prostatic carcinoma (PC) cells in vitro to radiation (19). Additional studies have found a critical role for glutathione in mediating radiation resistance in prostate cancer (20,21). Intracellular redox status is often characterized by the ratio of reduced to oxidized glutathione, and decreasing this ratio in vitro (by addition of selenite) was found to radiosensitize prostate cancer cells. Elevated glutathione and other antioxidants seen in cancer are increasingly viewed as redox adaptation, which several new therapies aim to exploit, including the thiol-depleting agent TDZD-8 (4-benzyl-2-methyl-1,2,4-thiadiazolidine-3,5-dione) (22).

## MOTIVATION FOR HYPERPOLARIZED $^{13}$C MR IMAGING

The extraordinary technique hyperpolarized MR using DNP has the potential to revolutionize the way we use MR imaging in the risk assessment of prostate cancer patients. In particular, hyperpolarization addresses some of the intrinsic limitations of $^{1}$H MRS, including low sensitivity, overlap of key resonances, and lack of information about metabolic fluxes. Hyperpolarized $^{13}$C methodology is based on polarizing nuclear spins in an amorphous solid state at approximately 1.2 K through coupling of the nuclear spins with unpaired electrons that are added to the sample via an organic free radical. In the solid state, the high-electron-spin polarization is in part transferred to the nuclear spins by microwave irradiation, and then the sample is rapidly dissolved for injection into a system of interest (23). $^{13}$C-labeled substrates have been recently polarized to obtain dramatic enhancements of the $^{13}$C NMR signals (>50,000-fold at 3-T) of the substrate as well as subsequent

metabolic products. The enhancement that is achieved is lost in time as a function of the spin-lattice relaxation time of the nucleus ($T_1$).

Several of the previously discussed metabolic shifts have been explored using hyperpolarized MR methods. Specifically, the glycolytic phenotype has been interrogated by hyperpolarized [U-$^{13}$C, U-$^{2}$H]glucose, hyperpolarized [2-$^{13}$C]fructose, hyperpolarized [1-$^{13}$C]pyruvate, hyperpolarized [1-$^{13}$C]lactate, and hyperpolarized [1-$^{13}$C]alanine (2). Hyperpolarized [1-$^{13}$C]pyruvate has been the most widely used probe for in vivo studies since it polarizes well, has a long $T_1$, is rapidly taken up by the cell, and is metabolized at the juncture of glycolysis, the tricarboxylic acid cycle, amino acid biosynthesis, and other critical pathways. Numerous hyperpolarized [1-$^{13}$C]pyruvate studies have been performed in transgenic and implanted tumors, perfused organs, and engineered cell systems, or bioreactors. Increased conversion of hyperpolarized [1-$^{13}$C]pyruvate to hyperpolarized [1-$^{13}$C]lactate has been detected in a variety of preclinical cancer models and found to correlate with tumor grade in a transgenic adenocarcinoma of the mouse prostate (TRAMP) model (24).

Probes to measure extracellular pH have also exploited the Warburg phenotype. As stated previously, acidification of the extracellular matrix is related, in part, to the export of excess lactic acid generated by aerobic glycolysis. The acidic tumor microenvironment may enhance both local invasion and distant spread of disease (metastases). Numerous other molecular imaging methods (including $^{31}$P MRS and PET-pHLIP [pH (low) insertion peptide]) have been developed to evaluate tumor acidity in vivo, but a recent promising method has used hyperpolarized $^{13}$C-bicarbonate. The interconversion of bicarbonate and $CO_2$ is facilitated by the family of carbonic anhydrases because the noncatalyzed rate of interconversion is slow relative to the metabolic fluxes. $^{13}$C-cesium bicarbonate was polarized by Gallagher et al., rapidly converted to $^{13}$C-sodium bicarbonate using an ion-exchange resin, and used to demonstrate cancer-catalyzed interconversion both in vitro and in tumor-bearing mice, demonstrating lower pH within tumor (25). The ratio of $^{13}$C-$HCO_3$ to $13CO_2$ is governed by the Henderson–Hasselbalch equation, and pH can readily be determined from integrating the corresponding resonances on a voxel-by-voxel basis. A subsequent study extended this approach to hyperpolarizing $^{13}$C-sodium bicarbonate itself and showing acidification of TRAMP tumors in a murine cohort (26).

Enriched glutamine is also readily polarized using the DNP technique, with hyperpolarized [5-$^{13}$C]glutamine and a partially deuterated version, hyperpolarized [5-$^{13}$C, 4-$^{2}H_2$]glutamine, both reported (27,28). The latter probe was designed to increase the apparent $T_1$ of the $^{13}$C nucleus, since this parameter determines a probe's useful hyperpolarized lifetime. Hyperpolarized glutamine has not yet been reported in conjunction with preclinical models of prostate cancer, but rapid glutaminolysis of the probe has been described in both human hepatocellular carcinoma and brain tumor cells.

The redox adaptation of tumors may be explored using approaches that target pools of intracellular antioxidants or, directly, reactive oxygen species. The former approach is highlighted by hyperpolarized [1-$^{13}$C]dehydroascorbate, the oxidized form of vitamin C, which is rapidly taken into cells by glucose transporters and reduced (29,30). This

conversion has been attributed to reduced glutathione, the principal small-molecule thiol antioxidant in cells. Reduction of hyperpolarized [1-$^{13}$C]dehydroascorbate takes place rapidly in the brain, liver, kidneys, and prostate tumor in the TRAMP model. Because the intracellular redox network is vast and complex, it is unlikely that this conversion is dependent solely on glutathione concentration or on the redox state of cells, often defined as the ratio of glutathione to oxidized glutathione. The exact mechanism of hyperpolarized [1-$^{13}$C]dehydroascorbate to hyperpolarized [1-$^{13}$C]vitamin C reduction is currently under investigation, but it appears likely that this conversion reflects the redox capacity of tissues in response to the oxidant stressor dehydroascorbate. Other approaches to imaging endogenous oxidizing species include hyperpolarized $^{13}$C-benzoylformic acid, which decomposes to a carboxylic acid ($^{13}$C-benzoic acid), a reaction readily observable by chemical shift (31). This method is far from clinical application but highlights the way hyperpolarized MR imaging may be used to target the chemical microenvironment of tumors.

## BEYOND MODELS: NEW METABOLIC PLATFORMS IN PROSTATE CANCER FOR HYPERPOLARIZED $^{13}$C MR

How well do commonly used prostate cancer models recapitulate the human condition? Unfortunately, testing of drugs using currently available preclinical models has not resulted in effective therapies in the clinic, and the dearth of relevant preclinical models has been identified as a limitation in the development of new cancer drugs. Preclinical prostate cancer models include monolayer primary and immortalized cell cultures, cocultures of stromal and epithelial cells, 3-dimensional cultures in matrices, and murine models of disease. The hyperpolarized $^{13}$C MR literature is biased toward animal models because of the interest in developing robust hardware, pulse sequences, and imaging protocols to prove that this nascent technology is readily clinically translatable. Transgenic models of prostate cancer include the TRAMP mouse and phosphatase and tensin homolog models, which recapitulate important features of human prostate cancer but have significant limitations. Limitations of these transgenic models include anatomic differences between the rodent and human gland, rapid progression to poorly differentiated cancer, absence of bony metastases, and lack of genetic heterogeneity, with oncogenes continuously “on” throughout the gland. These differences make it difficult to extend results obtained in transgenic models to human disease.

Frequently used prostate cancer cell cultures may also be inadequate to recapitulate human disease, as it is difficult to mimic the complex cell–cell and cell–matrix interactions found in normal tissue. These differences were highlighted by a recent study using primary human tissue slice cultures (TSCs) in an MR-compatible bioreactor. The study compared the metabolism of TSCs to snap-frozen, patient-derived prostate biopsy samples, 2 common immortalized prostate cancer cell-lines (PC-3 and VCaP), and primary prostate cancer cells using $^{1}$H high-resolution magic angle spinning (HR-MAS) spectroscopy (11). Snap-frozen patient-derived prostate biopsy samples were considered the gold standard, since these have been shown to best reflect the in vivo human prostate. The TSCs used were precision-cut from fresh tissues obtained at the time of surgery and cultured in a manner to provide

optimum nutrient and gas exchange. Steady-state concentrations of key metabolites were compared, in general demonstrating that TSCs showed similar $^{1}$H HR-MAS spectra to biopsy samples and that immortalized cancer cell lines and primary cancer cells showed significant differences from both TSCs and biopsies. These data are summarized in Figure 2A. The first observation is related to citrate and polyamine resonances, hallmarks of prostate metabolism seen by in vivo $^{1}$H MRS. These metabolites were not detected in the immortalized cell lines or primary prostate cancer cells but were found in the biopsy samples and TSCs. Of note, citrate levels were found to be lower in the TSCs than in biopsy samples, possibly because of the different treatment of the tissues before $^{1}$H HR-MAS (snap freezing vs. incubation in medium). Second, lactate found in TSCs was on the same order as their biopsy counterparts, with much higher levels found in PC-3, VCaP, and primary prostate cancer cells. Third, the steady-state glutamate concentrations were similar in TSCs and biopsy samples, although dramatically different from PC3 and primary cells (higher) and VCaP cells (lower). Finally, for PC3 cells choline metabolism differed significantly from the other tissues and cells studied. These experiments highlighted the perils of translating data obtained in cell cultures to the clinic. In particular, the metabolic signatures of primary cell cultures did not recapitulate those found in biopsy samples, which may reflect selection of the most aggressive cell phenotypes in culture. Furthermore, these studies suggested that the TSC platform may better approximate the human condition than other available culture models. Bioreactor-loaded TSCs were further interrogated with hyperpolarized [1-$^{13}$C]pyruvate, demonstrating increased pyruvate-to-lactate flux that correlated with lactate dehydrogenase and monocarboxylate transporter expression (Fig. 2B). These methods may be further extended to biopsy samples themselves, with a potentially profound impact on patient care.

## HYPERPOLARIZED $^{13}$C MR IMAGING IN PROSTATE CANCER PATIENTS

A decade after the first demonstration of dissolution-DNP by Ardenkjaer-Larsen et al. (23), metabolic imaging using hyperpolarized [1-$^{13}$C]pyruvate was accomplished in prostate cancer patients at the University of California San Francisco (1). Importantly, this study showed that injection of hyperpolarized [1-$^{13}$C]pyruvate was safe in 31 patients with biopsy-proven localized prostate cancer with a median age of 63 y. Safety was important to establish, given the difference in pharmacologic dose between $^{13}$C hyperpolarized MR and other metabolic imaging technologies such as PET (the difference between hyperpolarized [1-$^{13}$C]pyruvate and $^{18}$F-FDG doses is on the order of $10^{7}$). Both 2-dimensional dynamic MRSI and single-time-point MRSI were demonstrated, showing that in many cases the observed hyperpolarized [1-$^{13}$C] lactate metabolite accurately reflected the presence, location, and size of cancer relative to surrounding benign tissues. A study performed using the highest hyperpolarized [1-$^{13}$C]pyruvate dose is depicted in Figure 3. Significantly, in several cases hyperpolarized $^{13}$C MRS revealed regions of the prostate that were previously missed by state-of-the-art $^{1}$H multiparametric imaging that was performed as part of the clinical trial. This study was highly promising and demonstrated the potential to use hyperpolarized MR in a variety of clinical contexts with altered glycolysis.

## THE FUTURE

The development of rapid-dissolution DNP methods has, in a short time, afforded profound insights into prostate cancer metabolism. These insights have been obtained largely in pre-clinical disease models, which recapitulate several of the key metabolic shifts found in cancer, namely accelerated glycolysis, glutamine consumption, and redox adaptation. Metabolic studies using both $^{1}H$ and hyperpolarized $^{13}C$ spectroscopy have reinforced the view that these models need to better recapitulate human in vivo prostate cancer, to provide an appropriate platform for biomarker identification and validation. We anticipate that miniaturization of perfused cellular systems will allow rapid metabolic characterization of human biopsy samples, with the goal of tailoring therapy to individual patient phenotypes.

Although miniaturization is a significant goal in the metabolic analysis of ex vivo samples, adaptation of preclinical hyperpolarized MRS methods to humans requires significant innovation. As the recent clinical trial using hyperpolarized [1-$^{13}C$]pyruvate suggests, several of these challenges have already been met. Future efforts in humans will be driven by new hyperpolarized probes, improved methods for polarization and delivery of $^{13}C$ substrates, MR pulse sequences using sparse sampling techniques, parallel imaging methodologies, and improved coil design. Importantly, continued attention to biochemical detail will be needed to establish the clinical value of hyperpolarized $^{13}C$ MRS alongside existing $^{1}H$ methods in the multiparametric prostate MR examination.

## References


1. Nelson SJ, Kurhanewicz J, Vigneron DB, et al. Metabolic imaging of patients with prostate cancer using hyperpolarized [1-$^{13}C$]pyruvate. Sci Transl Med. 2013; 5:198ra108.
2. Keshari KR, Wilson DM. Chemistry and biochemistry of $^{13}C$ hyperpolarized magnetic resonance using dynamic nuclear polarization. Chem Soc Rev. 2014; 43:1627–1659. [PubMed: 24363044]
3. Siegel R, Ma J, Zou Z, Jemal A. Cancer statistics, 2014. CA Cancer J Clin. 2014; 64:9–29. [PubMed: 24399786]
4. Scher HI, Fizazi K, Saad F, et al. Increased survival with enzalutamide in prostate cancer after chemotherapy. N Engl J Med. 2012; 367:1187–1197. [PubMed: 22894553]
5. Ryan CJ, Smith MR, de Bono JS, et al. Abiraterone in metastatic prostate cancer without previous chemotherapy. N Engl J Med. 2013; 368:138–148. [PubMed: 23228172]
6. Palmgren JS, Karavadia SS, Wakefield MR. Unusual and underappreciated: small cell carcinoma of the prostate. Semin Oncol. 2007; 34:22–29. [PubMed: 17270662]
7. Beltran H, Tagawa ST, Park K, et al. Challenges in recognizing treatment-related neuroendocrine prostate cancer. J Clin Oncol. 2012; 30:e386–e389. [PubMed: 23169519]
8. Coller HA. Is cancer a metabolic disease? Am J Pathol. 2014; 184:4–17. [PubMed: 24139946]
9. Singh KK, Desouki MM, Franklin RB, Costello LC. Mitochondrial aconitase and citrate metabolism in malignant and nonmalignant human prostate tissues. Mol Cancer. 2006; 5:14. [PubMed: 16595004]
10. Glunde K, Bhujwalla ZM, Ronen SM. Choline metabolism in malignant transformation. Nat Rev Cancer. 2011; 11:835–848. [PubMed: 22089420]
11. Keshari KR, Sriram R, Van Criekinge M, et al. Metabolic reprogramming and validation of hyperpolarized $^{13}C$ lactate as a prostate cancer biomarker using a human prostate tissue slice culture bioreactor. Prostate. 2013; 73:1171–1181. [PubMed: 23532911]
12. Keshari KR, Sriram R, Koelsch BL, et al. Hyperpolarized $^{13}C$-pyruvate magnetic resonance reveals rapid lactate export in metastatic renal cell carcinomas. Cancer Res. 2013; 73:529–538. [PubMed: 23204238]

13. Fantin VR, St-Pierre J, Leder P. Attenuation of LDH-A expression uncovers a link between glycolysis, mitochondrial physiology, and tumor maintenance. Cancer Cell. 2006; 9:425–434. [PubMed: 16766262]
14. Wise DR, DeBerardinis RJ, Mancuso A, et al. Myc regulates a transcriptional program that stimulates mitochondrial glutaminolysis and leads to glutamine addiction. Proc Natl Acad Sci USA. 2008; 105:18782–18787. [PubMed: 19033189]
15. Gao P, Tchernyshyov I, Chang TC, et al. c-Myc suppression of miR-23a/b enhances mitochondrial glutaminase expression and glutamine metabolism. Nature. 2009; 458:762–765. [PubMed: 19219026]
16. Al-Mamgani A, Lebesque JV, Heemsbergen WD, et al. Controversies in the treatment of high-risk prostate cancer: what is the optimal combination of hormonal therapy and radiotherapy: a review of literature. Prostate. 2010; 70:701–709. [PubMed: 20017166]
17. Nichol AM, Warde P, Bristow RG. Optimal treatment of intermediate-risk prostate carcinoma with radiotherapy: clinical and translational issues. Cancer. 2005; 104:891–905. [PubMed: 16007687]
18. Sun Y, St Clair DK, Xu Y, Crooks PA, St Clair WH. A NADPH oxidase-dependent redox signaling pathway mediates the selective radiosensitization effect of parthenolide in prostate cancer cells. Cancer Res. 2010; 70:2880–2890. [PubMed: 20233868]
19. Lu JP, Monardo L, Bryskin I, et al. Androgens induce oxidative stress and radiation resistance in prostate cancer cells though NADPH oxidase. Prostate Cancer Prostatic Dis. 2010; 13:39–46. [PubMed: 19546883]
20. Husbeck B, Peehl DM, Knox SJ. Redox modulation of human prostate carcinoma cells by selenite increases radiation-induced cell killing. Free Radic Biol Med. 2005; 38:50–57. [PubMed: 15589371]
21. Sainz RM, Reiter RJ, Tan DX, et al. Critical role of glutathione in melatonin enhancement of tumor necrosis factor and ionizing radiation-induced apoptosis in prostate cancer cells in vitro. J Pineal Res. 2008; 45:258–270. [PubMed: 18384530]
22. Trachootham D, Alexandre J, Huang P. Targeting cancer cells by ROS-mediated mechanisms: a radical therapeutic approach? Nat Rev Drug Discov. 2009; 8:579–591. [PubMed: 19478820]
23. Ardenkjaer-Larsen JH, Fridlund B, Gram A, et al. Increase in signal-to-noise ratio of > 10,000 times in liquid-state NMR. Proc Natl Acad Sci USA. 2003; 100:10158–10163. [PubMed: 12930897]
24. Albers MJ, Bok R, Chen AP, et al. Hyperpolarized $^{13}$C lactate, pyruvate, and alanine: noninvasive biomarkers for prostate cancer detection and grading. Cancer Res. 2008; 68:8607–8615. [PubMed: 18922937]
25. Gallagher FA, Kettunen MI, Day SE, et al. Magnetic resonance imaging of pH in vivo using hyperpolarized $^{13}$C-labelled bicarbonate. Nature. 2008; 453:940–943. [PubMed: 18509335]
26. Wilson DM, Keshari KR, Larson PE, et al. Multi-compound polarization by DNP allows simultaneous assessment of multiple enzymatic activities in vivo. J Magn Reson. 2010; 205:141–147. [PubMed: 20478721]
27. Gallagher FA, Kettunen MI, Day SE, Lerche M, Brindle KM. $^{13}$C MR spectroscopy measurements of glutaminase activity in human hepatocellular carcinoma cells using hyperpolarized $^{13}$C-labeled glutamine. Magn Reson Med. 2008; 60:253–257. [PubMed: 18666104]
28. Qu W, Zha Z, Lieberman BP, et al. Facile synthesis [5-$^{13}$C-4-$^{2}H_2$]-L-glutamine for hyperpolarized MRS imaging of cancer cell metabolism. Acad Radiol. 2011; 18:932–939. [PubMed: 21658976]
29. Keshari KR, Kurhanewicz J, Bok R, Larson PE, Vigneron DB, Wilson DM. Hyperpolarized $^{13}$C dehydroascorbate as an endogenous redox sensor for in vivo metabolic imaging. Proc Natl Acad Sci USA. 2011; 108:18606–18611. [PubMed: 22042839]
30. Bohndiek SE, Kettunen MI, Hu DE, et al. Hyperpolarized [1-$^{13}$C]-ascorbic and dehydroascorbic acid: vitamin C as a probe for imaging redox status in vivo. J Am Chem Soc. 2011; 133:11795–11801. [PubMed: 21692446]
31. Lippert AR, Keshari KR, Kurhanewicz J, Chang CJ. A hydrogen peroxide-responsive hyperpolarized $^{13}$C MRI contrast agent. J Am Chem Soc. 2011; 133:3776–3779. [PubMed: 21366297]

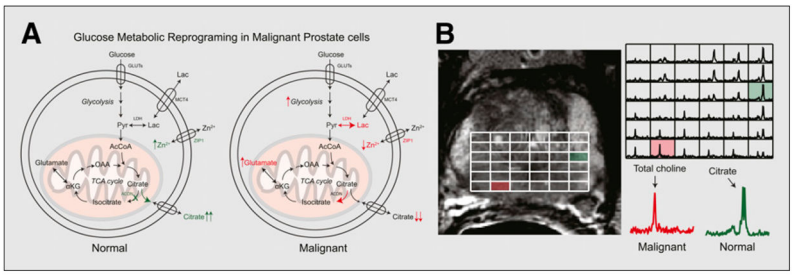


**FIGURE 1.**

Metabolic reprogramming in prostate cancer, observed by $^{1}$H MRS. (A) Change in glucose metabolism when comparing normal prostate glandular epithelial cells and malignant prostate cells. (B) Representative T2-weighted imaging and corresponding 3-dimensional MRSI array in patient with Gleason 3 + 4 cancer in right base of prostate gland. Inlaid spectra corresponding to normal and malignant voxel demonstrate differences in metabolism for these regions, with large citrate resonance observed in normal prostate tissue and abnormal choline peak in cancer. GLUTs = glucose transporters; ZIP1 = zinc transporter; AcCoA = acetyl-CoA; ACCH = acetylcholine; αKG = α-ketoglutarate; Lac = lactate; LDH = lactate dehydrogenase; MCT4 = monocarboxylate transporter 4; OAA = oxaloacetate; Pyr = pyruvate; TCA = tricarboxylic acid.

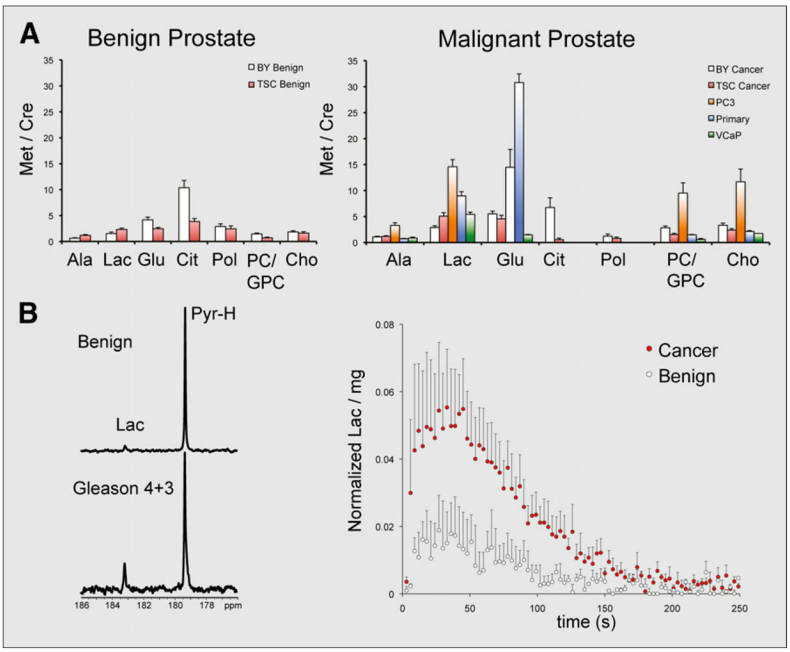


**FIGURE 2.**

Spectroscopic studies demonstrate challenges of studying metabolism using cells in culture and validate tissue slices (TSCs) as platform for hyperpolarized $^{13}C$ research. (A) Quantified metabolite ratios for benign and malignant prostate tissues, obtained using $^{1}H$ HR-MAS. Differences in metabolite ratios between TSCs and snap-frozen biopsy samples are compared, as well as those obtained from primary prostate cancer cells and immortalized cell lines PC3 and VCap. (B) Metabolic study of TSCs on bioreactor platform using hyperpolarized [1-$^{13}C$] pyruvate. Both single spectrum acquired at 90 s and normalized dynamic data show significantly increased conversion to hyperpolarized [1-$^{13}C$]lactate in malignant TSCs. Ala = alanine; BY = biopsy samples; Cho = choline; Cit = citrate; Glu = glutamic acid; GPC = glycerophosphocholine; Lac = lactate; Pol = polyamines; Pyr = pyruvate.

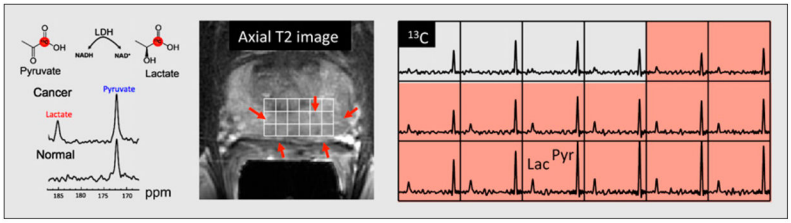


**FIGURE 3.**

Hyperpolarized $^{13}C$ MRS study in human patient with biopsyproven Gleason grade 3 + 3 prostate cancer using 3-dimensional MRSI at a single time point. This patient received highest dose of hyperpolarized [1-$^{13}C$]pyruvate (0.43 mL/kg). Axial T2-weighted image through malignant region is juxtaposed with corresponding $^{13}C$ spectral array, with area of putative tumor highlighted by pink shading. Increased conversion to hyperpolarized [1-$^{13}C$]lactate was seen in this region, consistent with abnormalities found on multiparametric $^{1}H$ staging examination. Lac = lactate; Pyr = pyruvate; LDH = lactate dehydrogenase; NAD = nicotinamide adenine dinucleotide; NADH = reduced nicotinamide adenine dinucleotide.